Desalination and Water Treatment
www.deswater.com
doi: 10.5004/dwt.2022.28167

251 (2022) 105–113
March

Evaluation of the performance of an agricultural residue *Cyamopsis tetragonolobus* (guar gum) in toxic paint industry, effluent treatment using continuous fixed-bed adsorption column

S. Vishali*, S. Picasso, M. Rajdeep, B. Debom

Department of Chemical Engineering, College of Engineering and Technology, SRMIST Kattankulathur 603 203, Chennai, India, Tel. +91 94438 83562; emails: meet.vishali@gmail.com (S. Vishali), picassosengupta@gmail.com (S. Picasso), rjdp0494@gmail.com (M. Rajdeep), debombhattacherjee@gmail.com (B. Debom)

Received 17 September 2021; Accepted 12 January 2022

ABSTRACT

This study has been focused on the development of natural adsorbents for the decolorization of paint industry effluent. A natural residue *Cyamopsis tetragonolobus* (guar gum) was tested as an adsorbent in a fixed bed adsorption column. The design variables influent flow rate, adsorbent mass, effluent initial concentration were fixed as influencing parameters on the color removal. The adsorbent showcased its treatability at the lower initial concentration, lower flow rate and higher adsorbent mass. The adsorption phenomena were expressed using breakthrough curves and models. The transport of pollutants onto the adsorbent was explained with the help of mass transfer model equations. The results were recommended the usage of bio-based adsorbent *Cyamopsis tetragonolobus* (guar gum) for the decolorization of paint industry effluent.

Keywords: Paint industry effluent; Adsorption; *Cyamopsis tetragonolobus* (guar gum); Breakthrough models; Mass transfer models

1. Introduction

The presence of heavy metals, colorant, high biochemical oxygen demand/chemical oxygen demand, turbidity, total dissolved solids in the paint industry effluent converts it into a highly toxic pollutant, which defines that treatment before disposal is mandatory. Usually, the waste generated during the production of paint is much less (≈15%) than the waste generated from the degreasing of the unit operations (≈80%–85%). So the wastewater is a diluted form of paint only [1]. The complication involved in the treatment process depends on the origin of the solvent that existed in the effluent. Water-based effluents are usually simple to degrade than organic solvent-based paint effluent. The molecules of color, heavy metals released into the aquatic system damages not only the aquatic animal kingdom and also human health indirectly [2,3].

Largely to diminish the pollutants of lower concentration adsorption process would be suggested. The choice of adsorbent used depends on the availability and efficacy. In the process of pollutant removal from paint effluent, natural materials viz., *Strychnos potatorum*, *C. opuntia*, *Moringa oleifera*, *Cassia fistula* and the shells of shrimp, crab were attempted as a coagulant [4–6]. Besides immobilized packings of *Strychnos potatorum*, *C. opuntia*, *Portunus sanguinolentus* were also applied as adsorbents [7–9].

Different varieties of adsorbents in their natural form and also physically and chemically modified forms were utilized in the removal of dyes, heavy metals and organic and inorganic pollutants. The results were further motivated to search for a commercially viable and technically efficient adsorbent in the decolorization phenomena of paint industry effluent [10].

Guar gum has a molecular weight of about 220,000 and is constituted D-mannose, D-galactose as a straight chain

* Corresponding author.

Presented at the Virtual International Conference on New Strategies in Water Treatment and Desalination (WTD-2021), 21–23 March 2021, by SRM Institute of Science and Technology, Kattankulathur, India

and aside chain respectively in an alternative manner. Guar gum is the most widely used in the cosmetic industry, food industry, drug delivery, pharmacotherapy and water purification. Even though it is nonionic, it can be used as a flocculant in a wide range of pH and ionic strengths. Almost all the galactomannans are not soluble in organic solvents other than formamide. The most denoting solvent for galactomannans is water. In the dissolution process along with the hydration, it produces colloidal suspension with appreciable high viscous. Being a Non-Newtonian fluid it follows the pseudoplastic along growing shear rate. The viscosity of the guar gum solution is also inversely proportional to temperature. Guar gum solution is susceptible to microbial decay biocompatible. If not used within 24 h, the unpreserved guar gum solution must be preserved with preservatives [11–16].

The application of guar gum as an adsorbent on the treatment of paint industry effluent is not attempted yet. Keeping this gap in our mind, this research was focused to find the optimized conditions to decolorize the paint industry effluent using *Cyamopsis tetragonoloba* immobilized beads as packing in an adsorption column by modifying the operational parameters viz., initial effluent concentration, flow rate and packing length.

2. Materials and methods

2.1. Materials

2.1.1. Adsorbate

The adsorbate selected for the current study was water based paint wastewater (WPW). It was prepared by mixing white primer and blue colorant at the proportion of 4% (wt./vol.). The samples of different initial concentrations such as 1,250; 2,000 and 3,100 mg/L were prepared and used (Table 1) [9]. The physic-chemical properties are listed in Table 2 [17].

2.1.2. Adsorbent

Seeds of *Cyamopsis tetragonolobus* (guar gum) were procured from a seed shop in Pudukottai, Tamil Nadu, India. Using the domestic blender it was crushed towards powder and brought to 0.5 mm size using sieves.

2.1.3. Fixed bed column

Pyrex glass was used to fabricate a fixed-bed column (FBC) with an inner diameter of 2 cm and a length of 50 cm with a tapered end (Fig. 2). A peristaltic pump (Ravel Hitek, India) with a managed flow rate was used to pump wastewater into an FBC from the top at N.T.P. conditions [18].

Table 1
Concentration of WPW (made upto 1,000 mL)

Sample number	White primer (mL)	Blue colorant (mL)	Initial chemical oxygen demand (mg/L)
1	48	2	1,250
2	44	6	2,000
3	40	10	3,100

2.2. Methods

2.2.1. Preparation of encapsulated beads

The encapsulation of *Cyamopsis tetragonolobus* was carried out with the help of the sodium alginate component. Using a magnetic stirrer with a hot plate, *Cyamopsis tetragonolobus* powder (3% (w/v)) and sodium alginate (1% (w/v)) were suspended in distilled water. Hot temperatures (≤45°C) being maintained to guarantee consistent mixing without any lumps. When the temperature is elevated, the adsorbent's characteristics may be lost. Using a syringe, the resulting combination was ejected as a dewdrop in an antiseptic $CaCl_2$ solution (3%) at 25°C. The encapsulated pellets were strengthened by soaking them in a new $CaCl_2$ solution at 4°C for overnight and then rinsing them with deionized water to remove any excess calcium ions. As a control, encapsulated beads were created entirely from sodium alginate [8].

Using the volume displacement approach, the mean diameter of the immobilized bead was determined to be 0.53 cm. The density of beads (ρ) 0.75 g/cc was computed by dividing the mass of a known number of beads by total volume. The adsorbent's bulk density (ρ_B) was calculated by dividing the total mass of the beads used for the requisite packing height by the volume of the beads, and the conclusion was 0.856 g/cc.

2.2.2. Experimental set-up

In a FBC, the arrangements were made from the bottom as, glass wool, glass beads, encapsulated *Cyamopsis tetragonolobus* pellets and glass beads. The glass beads served as a supporting layer, and glass wool was used to minimize the glass beads from being jammed in the outlet. The glass beads at the top are there to ensure a seamless input flow. The adsorbate was fed in a down flow mode at a controlled flow rate and a room temperature of 30°C without any pH adjustment.

The packing of the beads began with half-filled distilled water in a fixed bed column, followed by the gentle addition of a known mass of beads. For each run, almost constant and uniform packing was accomplished according to

Table 2
Physico-chemical characteristics of the WPW (Sample number 3)

Parameters	Concentration (except for pH, color and turbidity)
pH at 25°C	7.7–8.1
Color, nm	Blue
Total dissolved solids, mg/L	214
Total suspended solids, mg/L	11,200
Oil and grease, mg/L	19
Chemical oxygen demand (COD), mg/L	3,100
Sulphate as SO_4, mg/L	24
Biochemical oxygen demand, mg/L (3 d incubated at 27°C)	1,375
Turbidity, NTU	1,780

the concept of terminal settling velocity. After achieving the appropriate bed height, the water was drained off, resulting in more tightened packing. The treated wastewater was collected regularly for residual color analysis.

The treatment was terminated once an FBC approached exhaustion point. The experiments were repeated three times to assure reproducibility. The given figures were based on the average of three different data sets. The trials were repeated to see how bed height, flow rate, and initial WPW concentration affected removal efficiency.

Once the column had acquired saturation stage, the treatment was discontinued. The experiments were run three times to assure stability. The presented data were the result of averaging three different data sets. The trials were repeated to see how bed height, flow rate, and WPW starting concentration affected removal efficiency [7–9].

2.2.3. Analysis

An SL 218 double UV-visible spectrophotometer (Elico-India) was used to examine the adsorbent's ability in the decolorization of SPIE at λ_{max} 612 nm.

3. Results and discussions

3.1. Effect of operating variables on breakthrough curves

3.1.1. Effect of initial effluent concentration

The initial concentration of the effluent described the pollutant load on it. The ability of the fabricated fixed-bed column in the removal of pollutant molecules is examined by varying the initial effluent concentration, whereas the bed height, flow rate were kept constant as 30 cm and 5 cc/min respectively. Three different initial concentration effluents viz., 1,250; 2,000 and 3,100 mg/L were applied. The process analysis parameters of an FBC are given in Table 3.

The observations from Fig. 1 and Table 4 indicated that the increase in the pollutant load shortened the breakthrough time (from 40 to 10 min) and total time (from 200 to 170 min). A known height of adsorbent packings was deactivated and saturated faster for the higher concentrations, which brought down the breakthrough time and the total time.

For the given system, a liter of 1,250 mg/L initial concentration effluent could be treated whereas only 850 mL of 3,100 mg/L loads of effluent were treated. The phenomena indicate that when the total treatment time extends it could treat more volume of effluent. The raise in the q_t value (7.45–11.24 mg/g) corresponding to the effluent concentration revealed the transportation of the pollutants onto the adsorbent [19,20].

3.1.2. Effect of adsorbent packing height

The success of the adsorption treatment process in primarily depends on the selection of an adsorbent and the availability of the required amount of adsorbent. Here the phrase "packing height" refers to the amount of adsorbent used, which linearly determines the number of active sites

Table 3
Process analysis parameters of a FBC

Total quantity of solute adsorbed for a given C_o, Q, mg	$q_t = QC_o\int_0^{t_t}\left(1-\frac{C_t}{C_o}\right)dt$
Volume of effluent treated, mL	$V_{\text{eff}} = Qt_t$
Empty bed residence time (EBRT), min	Bedvolume / Volumetric flowrate of the effluent
Mass transfer zone or equivalent length of unused bed (MTZ), cm	$H\left(1-\frac{t_b}{t_s}\right)$

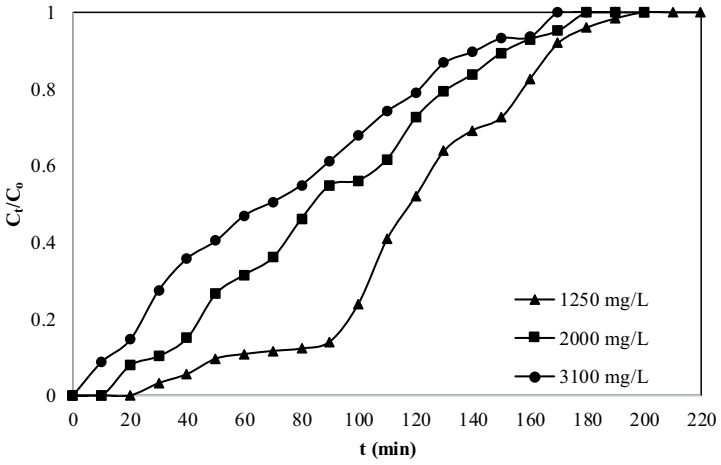

Fig. 1. Effect of initial effluent concentration on breakthrough curves.

available. Unsatisfactory results may occur due to a lack of bed height.

The success of the adsorption treatment process primarily depends on the selection of an adsorbent and the availability of the required amount of adsorbent. Here the phrase "packing height" refers to the amount of adsorbent used, which linearly determines the number of active sites available. Unsatisfactory results may occur due to a lack of bed height.

The time it took to achieve equilibrium removal in 10 cm to 30 cm columns made from encapsulated *Cyamopsis tetragonolobus* beads was 90, 130 and 160 min (Fig. 2). Under these settings, the breakthrough times were the same for 10 and 20 cm heights, but it is 40 min for 30 cm packing height. When the adsorbent bed height was increased, adsorption capacities (q_t) were climbed from 3.24 to 7.45 mg/g, while the length of the mass transfer zone increased from 8.89 cm to 22.50 cm, all following the same pattern. Similarly, the treated effluent volume increased from 0.5 to 1 L (Table 4).

Furthermore, as bed height increased, the slope of the breakthrough curve became flatter, resulting in a wider mass transfer zone (8.89–22.50 cm). The slope of the breakthrough curve reduced as bed height increased, owing to the increased availability of adsorbate–adsorbent contact time, which boosted removal capacity and decreased solute content in the effluent [21].

3.1.3. Effect of effluent flow rate

As the flow rate increased from 5 to 15 mL/min, the overall time taken to complete each run decreased. For the applied flow rates the total time and breakthrough time were 200, 140 and 100 min and 40, 10 and 10 min, respectively. With a higher flow rate, the breakthrough curves were steeper and faster. The empty bed residence time dropped from 31.4 to 10.5 min. From 1 to 1.5 L, the total volume of the treated effluent grown substantially (Fig. 3 and Table 4).

The color uptake was higher in the onset, then dropped significantly until saturation was approached. The contract duration was stretched by lowering the flow rate, while the adsorption zone was shortened. The ion exchange situation vary when the volumetric flow rate was reduced from 15 to 5 mL/min. When the flow rate was increased, the breakthrough curves became steeper and reached the breakthrough point in a shorter time. This could be because (a) the bed's saturation capacity was set to allow for concentration changes and (b) despite the high flow rate, adsorption equilibrium could be achieved due to the long residence time of the adsorbate in the column. At greater flow rates, the contact period between pollutant and adsorbent was fairly short, resulting in a decrease in removal efficiency [22].

To recap, the adsorbent acquired saturated quickly at a higher linear flow rate because brief contact time resulted

Table 4
Influence of operating variables on a FBC design parameters

C_o	Q	H	t_t	q_t	t_b	t_s	V_{eff}	EBRT	MTZ
mg/L	cc/min	cm	min	mg/g	min	min	mL	min	cm
1,250	5	10	100	3.24	10	90	500	31.4	8.89
1,250	5	20	140	4.93	10	130	700	31.4	18.46
1,250	5	30	200	7.45	40	160	1,000	31.4	22.50
1,250	10	30	140	10.1	10	130	1,400	15.7	27.69
1,250	15	30	100	8.33	10	90	1,500	10.47	26.67
2,000	5	30	180	8.91	20	160	900	31.4	26.25
3,100	5	30	170	11.24	10	160	850	31.4	28.13

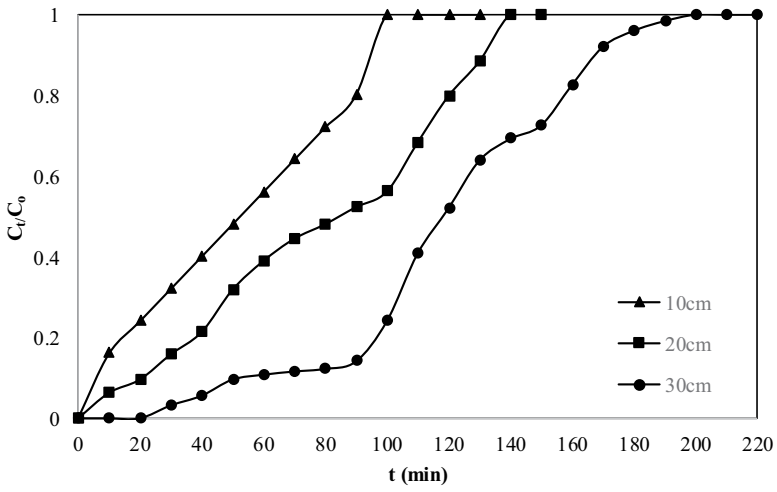

Fig. 2. Effect of adsorbent packing height on breakthrough curves.

in adsorption of a larger amount of pollutant on the adsorbent, resulting in weak diffusivity of the solute amidst the adsorbent particles [23].

3.2. Breakthrough curve models

Breakthrough curve models and their parameters have described the phenomena of the fixed bed continuous adsorption system. The linearized form of the models viz., Wang model, Thomas or bed depth service time (BDST) model, Yoon–Nelson model and Adams–Bohart model are tabulated in Table 5.

In the Wang model, the plot made between the ln[1/1–(C_t/C_o)] and time is shown in Fig. 4. The kinetic constant of Wang model k_W (0.0215 min^{-1}) and the time required to adsorb half of the initial concentration of the pollutants $t_{0.5}$ (62.47 min) are calculated using the slope and the intercept values of the plot and given in Table 6. The linear regression value is mentioned as 0.7774. The plot is made for the optimized parameters, but generally, the $t_{0.5}$ values would be in the increasing order concerning the ascending nature of pollutant load, due to the existence of a higher range of initial pollutant load [24]. The attained k_W value agrees with previous studies conducted on paint industry effluent using *Strychnos potatorum* [7].

Using the bed depth service time (BDST) model, the plot was drawn between ln[(C_o/C_t)–1] and time (Fig. 5). The model values k_{BDST} (kinetic constant), q_{BDST} (maximum adsorption capacity), were calculated and tabulated in Table 6. R^2 value (0.9604) was in good agreement with the linearity. The researchers found that the kinetic constant and the maximum adsorption capacity of the adsorbent were

Table 5
Breakthrough curve models for a FBC

Wang	$\ln\left[1/1-\left(C_t/C_o\right)\right]=-k_W t+k_W t_{0.5}$
BDST	$\ln\left[\left(C_o/C_t\right)-1\right]=\left(-k_{BDST}C_o\right)t+k_{BDST}q_{BDST}m/Q$
Yoon–Nelson model	$\ln\left(C_t/\left(C_o-C_t\right)\right)=k_{YN}t-k_{YN}\tau$
Adams–Bohart	$\ln\left(C_t/C_o\right)=\left(k_{AB}C_o\right)t-k_{AB}N_oH/U_o$

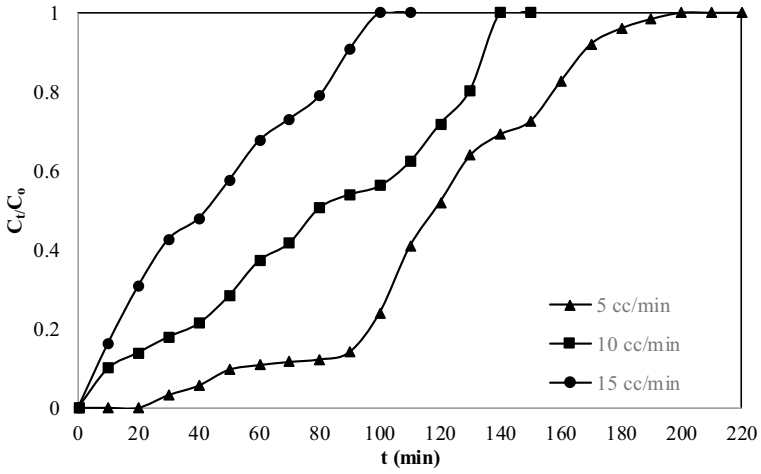

Fig. 3. Effect of effluent flow rate on breakthrough curves.

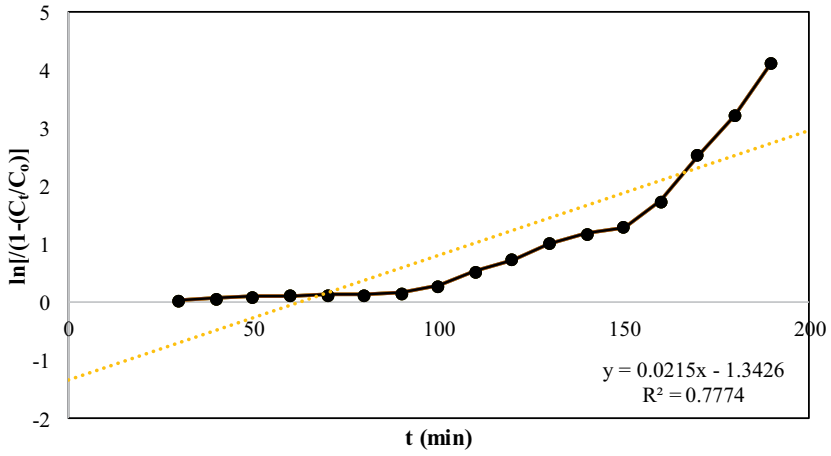

Fig. 4. Wang model curve under optimised conditions.

Table 6
Parameters of breakthrough models in a FBC at various conditions

C_o: 1,250 mg/L; Q: 5 cc/min; H: 30 cm			
Wang	k_W	1/min	0.0215
	$t_{0.5}$	min	62.47
	R^2		0.7774
BDST	k_{BDST}	L/(min mg)	3.432×10^{-5}
	q_{BDST}	mg/g	50,642
	R^2		0.9604
Yoon–Nelson	k_{YN}	1/min	0.0155
	τ	min	343.6
	R^2		0.7218
Adams–Bohart	k_{AB}	L/(min mg)	1.44×10^{-5}
	N_o	mg/L	2.645
	R^2		0.8969

inclined up with the increase in effluent entry flow rate, due to the higher mass of pollutant. For the fixed cross-sectional area of the adsorption column, according to the continuity equation of flow, the velocity of the effluent varies with flow rate [8].

The Yoon–Nelson model drawn for the breakthrough behavior of the treatment process uses $\ln[C_t/(C_o - C_t)]$ and time to determine k_{YN} and τ values (Fig. 6). Along with initial concentration, bed height the τ value also increased due to the higher mass gradient and more number of active sites respectively, whereas it showcased the declined trend with the rise in the flow rate because of the shortage in the residence time. The values found at the optimization conditions are listed in Table 6 [25].

Similarly, the Adams–Bohart model the rate constant k_{AB} (1.44×10^{-5} L/(min mg)), the maximum adsorption capacity per unit volume of adsorption column N_o (2.645 mg/L) were observed from the slope and the intercept of the plot made between $\ln C_t/C_o$ and time (Fig. 7) [26]. The values are

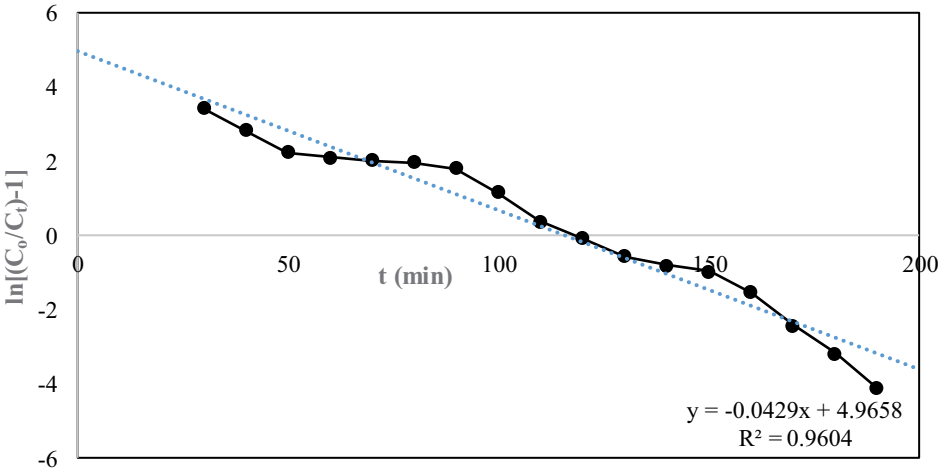

Fig. 5. BDST model curve under optimised conditions.

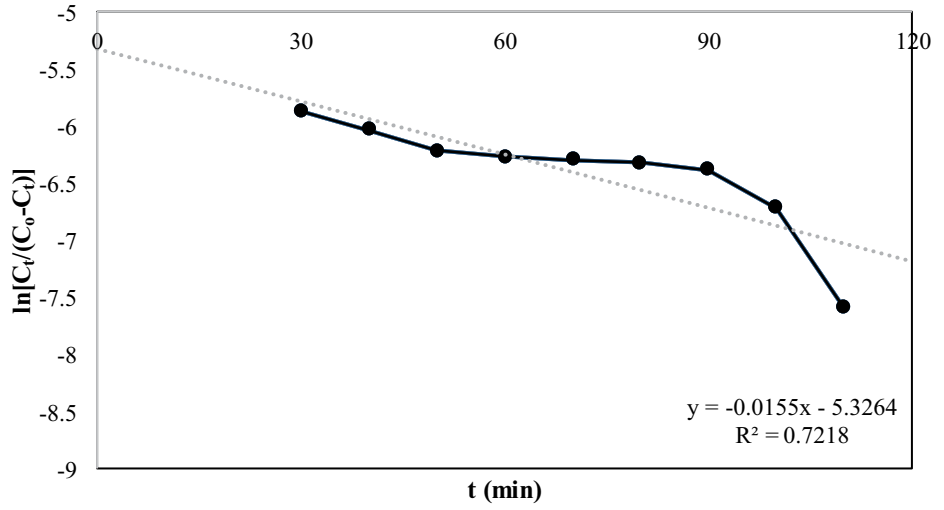

Fig. 6. Yoon–Nelson model curve under optimised conditions.

comparable with the studies done using *C. opuntia* on paint factory effluent and the trend varied based on the adsorbent origin [8].

3.3. Mass transfer model

The mass transfer may occur during the adsorption process, in addition to being adsorbed onto the surface of the adsorbent, due to intraparticle diffusion. The plot of the Weber–Morris model will not pass through the origin in this event, signaling that intraparticle diffusion was not the sole rate-controlling step and that film diffusion should not be ruled out as a rate-controlling feature. The k_{WM} (0.0578) values in this investigation indicated easier diffusion and transport into the pores of the adsorbents. The considerable intercept "*I*" (0.8878) also implied that the impacts on adsorbate mass transfer resistance were average growth, implying that external mass transfer resistance could not be ignored (Tables 7 and 8). The nonlinearity of the spots in Fig. 8 explains why the adsorption was determined by many processes. The solution is carried out by *I* an external diffusion mechanism, and (ii) intraparticle diffusion, based on the interception of the two lines. The linear regression coefficient is measured as 0.8969 [27,28].

The Mathews–Weber model could be used to determine the external mass transfer coefficients (2.04×10^{-5}) for adsorption. At the early contact time, it was believed that the concentration at the adsorbent surface tended toward zero and that intraparticle diffusion was insignificant. With high starting dye concentrations, the pollutant transport velocity from liquid to solid phase decreased, though intra-particle diffusion increased. The linear regression coefficient is measured as 0.8969 (Fig. 9 and Tables 7, 8) [29].

4. Conclusions

From the commenced research studies it was noticed that the *Cyamopsis tetragonoloba* could be recognized as a novel plant-based adsorbent in the decolorization of paint industry effluent. The immobilized beads of *Cyamopsis tetragonoloba* with a packing height of 30 cm in the 2 cm diameter fixed-bed column, with a flow rate of 5 mL/min yielded the better removal efficiency for the 1,250 mg/L initial concentration SPIE at room temperature. For the recommended conditions the break-through behavior, equilibrium pollutant uptake, mass transfer zone, empty bed residence time and the total volume of effluent treated were evaluated. The process kinetic constant, maximum adsorption capacity, the time required for 50% adsorbate breakthrough time were found using the BDST model, Adams–Bohart, Yoon–Nelson and Wang model respectively. With the aid of the mass transfer model like Weber–Morris,

Table 7
Mass transfer models for a FBC

Weber–Morris	$q_t = k_{WM} t^{0.5} + I$
Mathews–Weber	$\ln(C_t / C_o) = (-k_{MW} a / V)t$; where $a / V = 6m / \rho_p d$

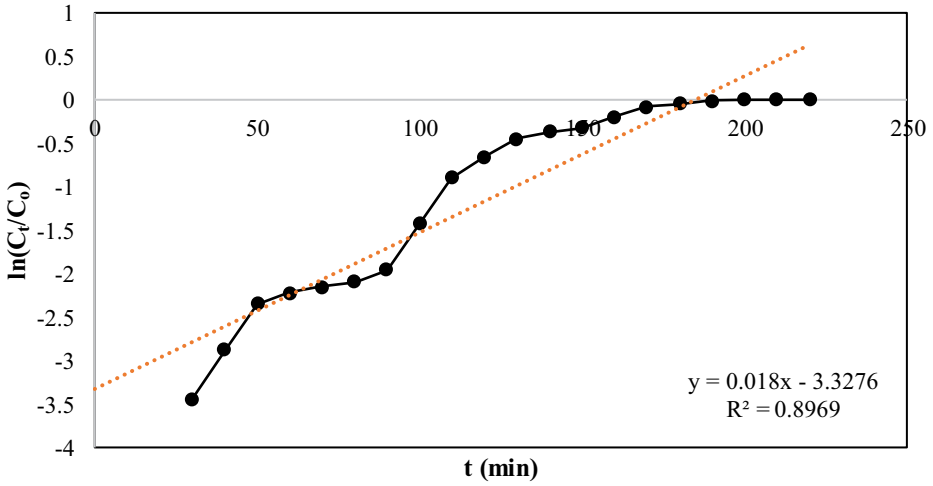

Fig. 7. Adams–Bohart model curve under optimised conditions.

Table 8
Parameters of mass transfer models in a FBC at various conditions

			Weber–Morris			Mathews–Weber	
C_o	Q	H	k_{WM}	I	R^2	k_{MW}	R^2
mg/L	cc/min	cm	mg/(min$^{0.5}$ g)			cm/min	
1,250	5	30	0.0578	0.8878	0.8288	2.04×10^{-5}	0.8969

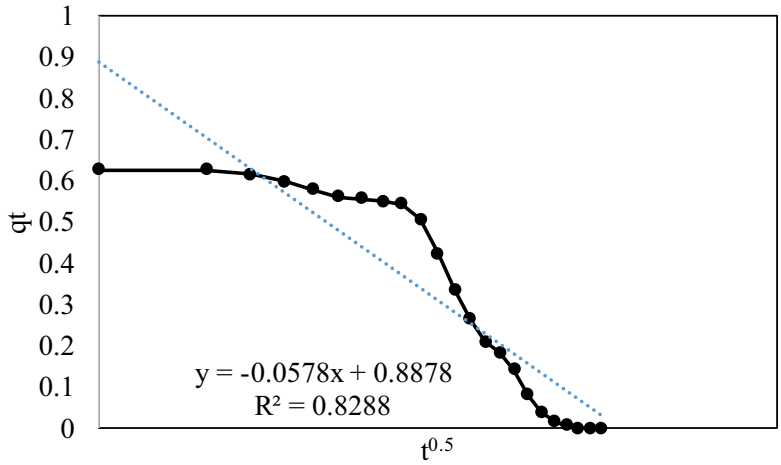

Fig. 8. Weber–Morris mass transfer model curve under optimised conditions.

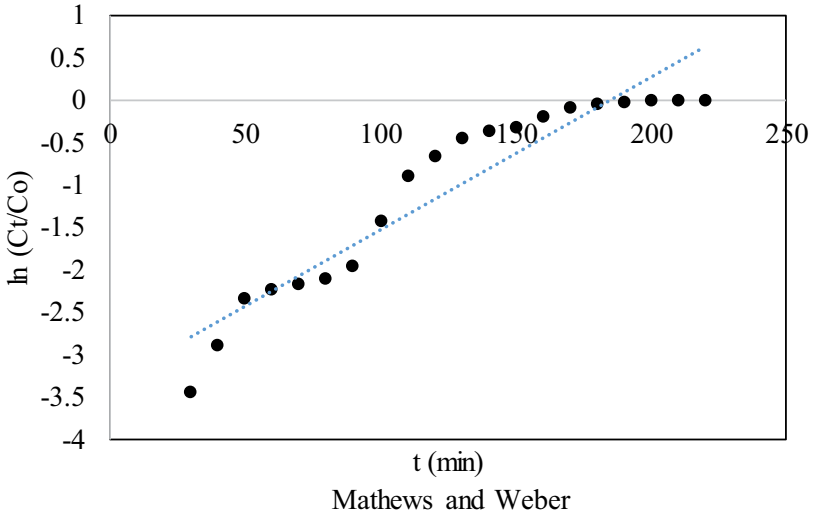

Fig. 9. Mathews–Weber mass transfer model curve under optimised conditions.

Mathews–Weber the transport behavior of the pollutant onto adsorbent was understood. As a summary, the results revealed that the potential of the *Cyamopsis tetragonoloba* as an adsorbent in the decolorization process was proved.

Symbols

a	—	Total interfacial area of particle, cm²
C_o, C_t	—	Concentration of the solute, and at time 't' in the effluent, mg/L
d	—	Mean diameter of immobilized beads, cm
H	—	Bed height, cm
I	—	Thickness of boundary layer, mg/g
k_{AB}	—	Kinetic constant in the model Adams–Bohart, L/(min mg)
k_{BDST}	—	Kinetic constant in the model BDST, L/(min mg)
k_{MW}	—	External mass transfer coefficient from Mathews–Weber model, cm/min
k_W	—	Kinetic constant in the model Wang, 1/min
k_{WM}	—	Kinetic constant in the model Weber–Morris, mg/(min$^{0.5}$ g)
k_{YN}	—	Kinetic constant in the model Yoon–Nelson, 1/min
m	—	Total mass of adsorbent, g
N_o	—	Maximum adsorption capacity per unit volume of adsorption column, mg/L
Q	—	Inlet feed flow rate, mL/min
q_{BDST}	—	Maximum adsorption capacity in BDST model, mg/g
q_t	—	Total quantity of pollutant adsorbed at time 't', mg/g
R^2	—	Correlation coefficient
t, t_b, t_s, t_t	—	Time, breakthrough time, saturation time, total time taken in FBC, min
$t_{0.5}$	—	Time required for 50% adsorbate breakthrough time, min
U_o	—	Linear velocity of inlet effluent, cm/min
V, V_{eff}	—	Volume of effluent, volume of effluent treated, mL

τ	—	Time required for 50% adsorbate breakthrough time in Yoon–Nelson model, min
ρ_P	—	Apparent density of the adsorbent, g/mL
ρ_B	—	Bulk density, g/mL

References

[1] B.K. Deya, M.A. Hashim, S. Hasan, B. Sen Gupta, Microfiltration of water-based paint effluents, Adv. Environ. Res., 8 (2004) 455–466.

[2] A. Akyol, Treatment of paint manufacturing wastewater by electrocoagulation, Desalination, 285 (2012) 91–99.

[3] D. Dursun, F. Sengul, Waste minimization study in a solvent-based paint manufacturing plant, Resour. Conserv. Recycl., 47 (2006) 316–331.

[4] S. Vishali, R. Karthikeyan, Application of green coagulants on paint industry effluent – a coagulation–flocculation kinetic study, Desal. Water Treat., 122 (2018) 112–123.

[5] S. Vishali, S. Sakthivel, R. Karthick, V.S. Gowsigan, A sustainable approach for the treatment of industrial effluent using a green coagulant *Cassia fistula* vs. chemical coagulant, Desal. Water Treat., 196 (2020) 189–197.

[6] S. Vishali, S. Picasso, M. Rajdeep, R. Nihal, Shrimp shell waste – a sustainable green solution in industrial effluent treatment, Desal. Water Treat., 104 (2018) 111–120.

[7] S. Vishali, P. Rashmi, R. Karthikeyan, Potential of environmental-friendly, agro-based material *Strychnos potatorum*, as an adsorbent, in the treatment of paint industry effluent, Desal. Water Treat., 57 (2016) 18326–18337.

[8] S. Vishali, P. Mullai, R. Karthikeyan, Breakthrough studies and mass transfer studies on the decolourization of paint industry wastewater using encapsulated beads of *Cactus opuntia* (*ficus-Indica*), Desal. Water Treat., 177 (2020) 89–101.

[9] S. Vishali, R. Karthikeyan, S. Prabhakar, Utilization of seafood processing waste, as an adsorbent, in the treatment of paint industry effluent using a fixed-bed column, Desal. Water Treat., 66 (2017) 149–157.

[10] J. QianJiang, S.M. Ashekuzzaman, Development of novel inorganic adsorbent for water treatment, Curr. Opin., 1 (2012) 191–199.

[11] S. Gaurav, S. Shweta, K. Amit, A.H.A. Muhtaseb, M. Naushad, A.A. Ghfar, G.T. Mola, F.J. Stadler, Guar gum and its composites as potential materials for diverse applications: a review, Carbohydr. Polym., 199 (2018) 534–545.

[12] B. Subhadeep, P. Anjali, Application of biopolymers as a new age sustainable material for surfactant adsorption: a brief review, Carbohydr. Polym., 2 (2021) 100145.

[13] N. Thombare, J. Usha, M. Sumit, M.Z. Siddiqui, Guar gum as a promising starting material for diverse applications: a review, Int. J. Biol. Macromol., 88 (2016) 361–372.

[14] S. Gaurav, K. Amit, D. Kunjana, S. Shweta, M. Naushad, A.A. Ghfar, T. Ahamad, Guar gum-crosslinked-Soya lecithin nanohydrogel sheets as effective adsorbent for the removal of thiophanate methyl fungicide, Int. J. Biol. Macromol., 114 (2018) 295–305.

[15] B. Jayachandrabal, S. Thirugnanasambandam, Ultrasound assisted synthesis of guar gum-zero valent iron nanocomposites as a novel catalyst for the treatment of pollutants, Carbohydr. Polym., 199 (2018) 41–50.

[16] T. Nandkishore, J. Usha, M. Sumit, M.Z. Siddiqui, Borax cross-linked guar gum hydrogels as potential adsorbents for water purification, Carbohydr. Polym., 168 (2017) 274–281.

[17] APHA, Standard Methods for the Examination of Waste and Wastewater, 16th ed., American Public Health Associations, New York, 1995.

[18] S. Vishali, J. Sandhiya, Divya, K. Aarthi, Abhilash, Performance evaluation of coconut shell originated activated carbon as an adsorbent on the paint factory effluent treatment, J. Phys. Conf. Ser., 2007 (2021) 012067.

[19] R. Kannan, S. Lakshmi, P. Radha, N. Aparna, S. Vishali, W. Richard Thilagaraj, Biosorption of heavy metals from actual electroplating wastewater using encapsulated *Moringa oleifera* beads in fixed bed column, Desal. Water Treat., 57 (2016) 3572–3587.

[20] Z.Z. Chowdhury, S.M. Zain, A.K. Rashid, R.F. Rafique, K. Khalid, Breakthrough curve analysis for column dynamics sorption of Mn(II) ions from wastewater by using *Mangostana garcinia* Peel-based granular-activated carbon, J. Chem., 2013 (2013) 959761, doi: 10.1155/2013/959761.

[21] J.T. Nwabanne, P.K. Igbokwe, Adsorption of packed bed column for the removal of lead(II) using oil palm fibre, Int. J. Appl. Sci. Technol., 2 (2012) 106–115.

[22] A.A. Ahmad, B.H. Hameed, Fixed bed adsorption of reactive azo dye onto granular activated carbon prepared from waste, J. Hazard. Mater., 175 (2010) 298–303.

[23] X. Luo, Z. Deng, X. Lin, C. Zhang, Fixed bed column study for Cu^{2+} removal from solution using expanding rice husk, J. Hazard. Mater., 187 (2011) 182–189.

[24] Y.H. Wang, S.H. Lin, R.S. Juang, Removal of heavy metal ions from aqueous solutions using various low-cost adsorbents, J. Hazard. Mater., 102 (2003) 291–302.

[25] Z. Xu, J.G. Cai, B.C. Pan, Mathematically modeling fixed-bed adsorption in aqueous systems, J. Zhejiang Univ. Sci. A, 14 (2013) 155–176.

[26] S. Zahra, S. Reyhane, F. Reza, Fixed-bed adsorption dynamics of Pb(II) adsorption from aqueous solution using nanostructured γ-alumina, J. Nanostruct. Chem., 3 (2013) 1–8.

[27] I.E. Hristova, Comparison of different kinetic models for adsorption of heavy metals onto activated carbon from apricot stones, Bulg. Chem. Commun., 43 (2011) 370–377.

[28] A.O. Okewale, K.A. Babayemi, A.P. Olalekan, Adsorption isotherms and kinetics models of starchy adsorbents on uptake of water from ethanol – water systems, Int. J. Appl. Sci. Technol., 3 (2013) 35–42.

[29] E.W. Bao, Y.H. Yong, X. Lei, P. Kang, Biosorption behavior of azo dye by inactive CMC immobilized *Aspergillus fumigates* beads, Bioresour. Technol., 99 (2008) 794–800.